

We are IntechOpen, the world's leading publisher of Open Access books Built by scientists, for scientists

6,900

Open access books available

186,000

International authors and editors

200M

Downloads

Our authors are among the

154

Countries delivered to

TOP 1%

most cited scientists

12.2%

Contributors from top 500 universities



WEB OF SCIENCE™

Selection of our books indexed in the Book Citation Index
in Web of Science™ Core Collection (BKCI)

Interested in publishing with us?
Contact book.department@intechopen.com

Numbers displayed above are based on latest data collected.
For more information visit www.intechopen.com



Design, Analysis and Applications of a Class of New 3-DOF Translational Parallel Manipulators

Yangmin Li and Qingsong Xu
*University of Macau,
 P. R. China*

1. Introduction

In recent years, the progress in the development of parallel manipulators has been accelerated since parallel manipulators possess many advantages over their serial counterparts in terms of high accuracy, velocity, stiffness, and payload capacity, therefore allowing their wide range of applications as industrial robots, flight simulators, parallel machine tools, and micro-manipulators, etc. Generally, a parallel manipulator consists of a mobile platform that is connected to a fixed base by several limbs or legs in parallel as its name implies (Merlet, 2000). Up to now, most 6-DOF parallel manipulators are based on the Gough-Stewart platform architecture due to the aforementioned advantages. However, six DOF is not always required in many situations. Besides, a general 6-DOF parallel manipulator has such additional disadvantages as complicated forward kinematics and excessive singularities within a relatively small size of workspace.

On the contrary, limited-DOF parallel manipulators with fewer than six DOF which not only maintain the inherent advantages of parallel mechanisms, but also possess several other advantages including the reduction of total cost of the device and control, are attracting attentions of various researchers. Many parallel manipulators with two to five DOF have been designed and investigated for pertinent applications. According to the properties of their output motion, the limited-DOF parallel manipulators can be classified into three categories in terms of translational, spherical, and mixed parallel manipulators. The first type allows the mobile platform a purely translational motion, which is useful as a machine tool, a positioner of an automatic assembly line, and so on. The second one enables the output platform only perform a rotational motion around a fixed point, and can be used in such situations as a telescope, an antenna, an end-effector of a robot, etc. And the last one allows the platform to both translate and rotate, and can be employed as a motion simulator, a mixed orientating/positioning tool, and others.

Particularly, due to the application requirements of translational motion, translational parallel manipulators (TPMs) become the focus of a great number of researches. The most well-known TPM is the Delta robot (Clavel, 1988) whose concept then has been realized in several different configurations (Tsai et al., 1996; Li & Xu, 2005), and many other structures have been also proposed in the literature. For example, the 3-UPU, 3-RUU and 3-PUU mechanisms (Tsai & Joshi, 2002), 3-RRC structure (Zhao & Huang, 2000), 3-RPC architecture (Callegari & Tarantini, 2003), 3-CRR manipulator (Kong & Gosselin, 2002; Kim & Tsai, 2003),

Source: Parallel Manipulators, New Developments, Book edited by: Jee-Hwan Ryu, ISBN 978-3-902613-20-2, pp. 498, April 2008, I-Tech Education and Publishing, Vienna, Austria

the Orthoglide (Chablat & Wenger, 2003), etc. Here the notation of R, P, U, and C denotes the revolute joint, prismatic joint, universal joint, and cylindrical joint, respectively. In addition, the recent advances in the systematic type synthesis of TPMs could be found in the literature (Kim & Chung, 2003; Kong & Gosselin, 2004).

It has been seen that most existing TPMs have a complex structure. Especially, some TPMs contain the U and S (spherical) joints which are not easy to manufacture and hence expensive although they are commercially available. From the economic point of view, the simpler of the architecture of a TPM is, the lower cost it will be spent. In previous works of the authors, two novel TPMs with the 3-PRC architecture have been proposed in (Li & Xu, 2006; Xu & Li, 2007). As an overconstrained mechanism, the 3-PRC TPM possesses a simpler structure than expected. However, the mobile platform has a relatively large dimension since the long C joints are mounted on it, which may prevent the TPM's applications in the situations where the mobile platform with a small size is preferred such as a pick-and-place operation over a limited space. In the current research, a new type of parallel mechanism called a 3-PCR TPM is proposed and investigated for various applications. With comparison to a 3-PRC TPM, the mobile platform of a 3-PCR TPM only contains the passive R joints, which allows the generation of a small size output platform accordingly.

The remainder of this chapter is organized in the following way. In section 2, the 3-PCR TPM architecture is described and the mobility is determined by resorting to the screw theory. Ant then, both the inverse and forward kinematics problems have been solved in Section 3, and the velocity equations are derived in Section 4. Next, four types of singular configurations are checked in Section 5, where the mechanism design rules to eliminate them are also given, and the isotropic configurations are derived in Section 6. Afterwards, the manipulator workspace has been obtained by both analytical and numerical approaches in Section 7, and the dexterity evaluations in terms of manipulability and global dexterity index have been carried out in Section 8. Then, in Section 9, the application of a 3-PCR TPM as a CPR medical robot has been proposed in detail, and several variation structures of the 3-PCR TPM have been presented in Section 10. Finally, some concluding remarks are given in Section 11.

2. Description and mobility analysis of the manipulator

2.1 Kinematical architecture

The CAD model of a 3-PCR TPM with intersecting guide ways is graphically shown in Fig. 1 and the schematic diagram is illustrated in Fig. 2, respectively. The TPM consists of a mobile platform, a fixed base, and three limbs with identical kinematical structure. Each limb connects the fixed base to the mobile platform through a P joint, a C joint, and an R joint in sequence, where the P joint is driven by a linear actuator mounted on the fixed base. Thus, the mobile platform is attached to the base by three identical PCR linkages. The following mobility analysis shows that in order to keep the mobile platform from changing its orientation, it is sufficient for the axes of passive joints within limbs to satisfy some certain geometric conditions. That is, the axes of the C and R joints within the same limb are parallel to each other.

The geometry of one typical kinematic chain is depicted in Fig. 3. To facilitate the analysis, as shown in Figs. 2 and 3, we assign a fixed Cartesian frame $O\{x, y, z\}$ at the centered point O of the fixed base, and a moving frame $P\{u, v, w\}$ on the triangle mobile platform at centered

point P , with the z - and w -axes perpendicular to the platform, x - and y -axes parallel to u - and v -axes, respectively.

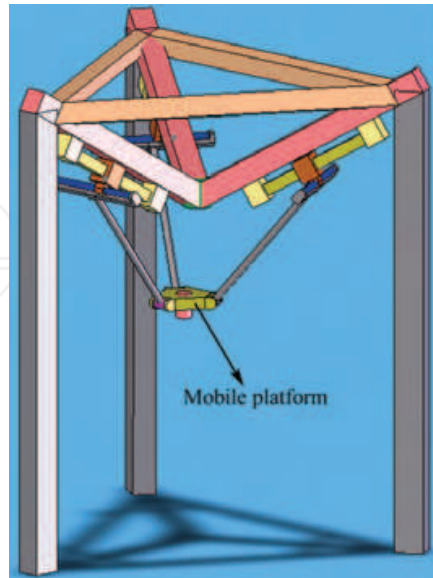


Fig. 1. A 3-PCR TPM with intersecting guide ways.

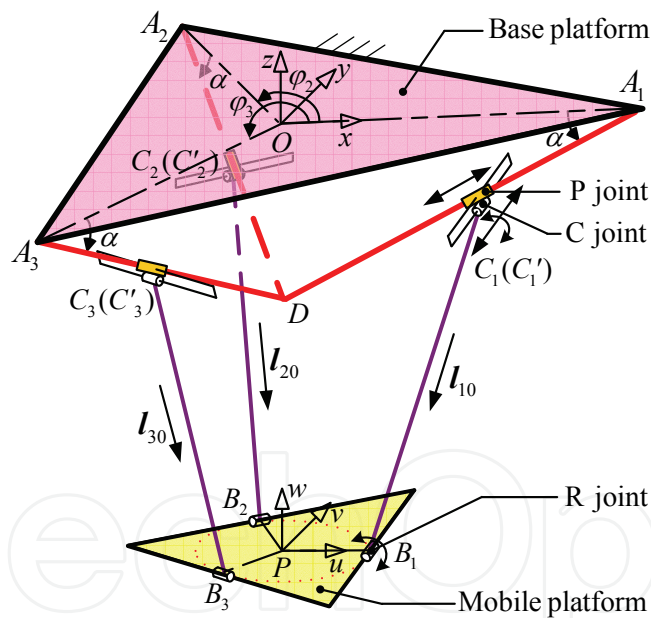


Fig. 2. Schematic diagram of a 3-PCR TPM.

The i -th limb C_iB_i ($i = 1, 2, 3$) with the length of l is connected to the passive C joint at C_i and connected to the mobile platform as point B_i . Q_i denotes the point on the C joint that is coincident with the initial position of C_i . And the three points B_i lie on a circle of radius b . In addition, the three rails M_iN_i intersect each other at point D and intersect the x - y plane at points A_1 , A_2 and A_3 respectively, that lie on a circle of radius a . The sliders of prismatic joints Q_i are restricted to move along the rails between M_i and N_i . Angle α is measured from the fixed base to rails M_iN_i and defined as the actuators layout angle. Without loss of generality, let the x -axis point along OA_1 and the u -axis direct along PB_1 . Angle φ_i is defined

some mechanisms but can not obtain the properties of the DOF, i.e., whether they are translational or rotational DOF.

On the contrary, we can effectively determine the mobility of a 3-PCR TPM by resorting to the screw theory (Hunt, 1990).

2.1.1 Overview of screw and reciprocal screw systems

In screw theory, a unit (normalized) screw is defined by a pair of vectors:

$$\hat{\$} = \begin{bmatrix} \mathbf{s} \\ \mathbf{r} \times \mathbf{s} + h\mathbf{s} \end{bmatrix} \quad (4)$$

where \mathbf{s} is a unit vector directing along the screw axis, \mathbf{r} denotes the position vector pointing from an arbitrary point on the screw axis to the origin of the reference frame, the vector $\mathbf{r} \times \mathbf{s}$ defines the moment of the screw axis with respect to the origin of the reference frame, and h represents the pitch of the screw. If the pitch equals to zero, the screw becomes:

$$\hat{\$} = \begin{bmatrix} \mathbf{s} \\ \mathbf{r} \times \mathbf{s} \end{bmatrix} \quad (5)$$

While in case of infinite pitch, the screw reduces to:

$$\hat{\$} = \begin{bmatrix} \mathbf{0} \\ \mathbf{s} \end{bmatrix} \quad (6)$$

A screw can be used to represent a twist or a wrench. With $\$F$ and $\$L$ respectively denoting the vectors of the first and last three components of a screw $\$$, then $\$F$ and $\$L$ respectively represent the angular and linear velocities when $\$$ refers to a twist, and the force and couple vectors when $\$$ refers to a wrench.

Two screws, namely, $\$r$ and $\$$, are said to be reciprocal if they satisfy the following condition.

$$\$r \circ \$ = [\tilde{\Delta}\$r]^T \$ = 0 \quad (7)$$

where “ \circ ” represents the reciprocal product operator, and the matrix $\tilde{\Delta}$, which is used to interchange the first and last three components of a screw ($\$r$), is defined by:

$$\tilde{\Delta} \equiv \begin{bmatrix} \mathbf{0} & \mathbf{I} \\ \mathbf{I} & \mathbf{0} \end{bmatrix} \quad (8)$$

where $\mathbf{0}$ and \mathbf{I} denote a zero matrix and an identity matrix in 3×3 , respectively. The physical meaning of reciprocal screws is that the wrench $\$r$ produces no work along the twist of $\$$.

Concerning an n -DOF spatial serial kinematic chain with n 1-DOF joints ($n \leq 6$), the joint screws (twists) associated with all the joints form an n -order twist system or n -system provided that the n joint screws are linearly independent. The instantaneous twists of the end-effector can be described as follows.

$$\mathcal{S} = \sum_{i=1}^n \dot{q}_i \hat{\mathcal{S}}_i \quad (9)$$

where \dot{q}_i is the intensity and $\hat{\mathcal{S}}_i$ is the unit screw associated with the i -th joint.

The reciprocal screw system of the twist system consists of $6-n$ linearly independent reciprocal screws (wrenches) and is called a $(6-n)$ -order wrench system or $(6-n)$ -system. In what follows, the relevant results of screw theory are utilized for the mobility investigation of a 3-PCR TPM.

2.1.2 Mobility determination of a 3-PCR TPM

For a 3-PCR parallel manipulator presented here, the motion of each limb that can be treated as a twist system is guaranteed under some exerted structural constraints which are termed as a wrench system. The wrench system is a reciprocal screw system of the twist system for the limb. The mobility of the manipulator is then determined by the effect of linear combination of the wrench systems for all limbs

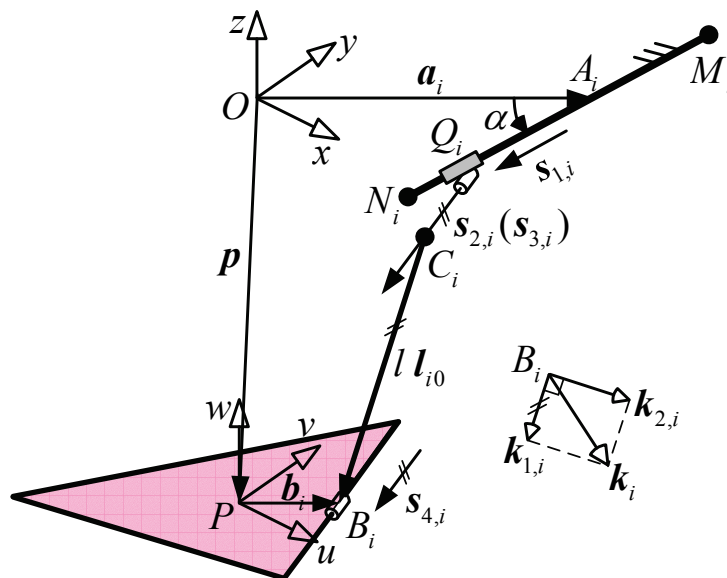


Fig. 4. Representation of screw vectors.

With $\omega = [\omega_x \ \omega_y \ \omega_z]^T$ and $v = [v_x \ v_y \ v_z]^T$ respectively denoting the vectors for the angular and linear velocities, then the twist of the mobile platform can be defined as $\mathcal{S}_p = [\omega^T \ v^T]^T$.

Considering that a C joint is equivalent to the combination of a P joint with a coaxial R joint, the connectivity of each limb for a 3-PCR TPM is equal to four since each limb consists of four 1-DOF joints. Hence, with reference to Fig. 4, the instantaneous twist \mathcal{S}_p of the mobile platform can be expressed as a linear combination of the four instantaneous twists, i.e.,

$$\mathcal{S}_p = \dot{d}_i \hat{\mathcal{S}}_{1,i} + \dot{\theta}_{2,i} \hat{\mathcal{S}}_{2,i} + \dot{\theta}_{3,i} \hat{\mathcal{S}}_{3,i} + \dot{s}_i \hat{\mathcal{S}}_{4,i} \quad (10)$$

for $i=1, 2, 3$, where $\dot{\theta}_{j,i}$ is the intensity and $\hat{\mathcal{S}}_{j,i}$ denotes a unit screw associated with the j -th joint of the i -th limb with respect to the instantaneous reference frame P , and

$$\hat{\mathbf{S}}_{1,i} = \begin{bmatrix} \mathbf{0} \\ \mathbf{s}_{1,i} \end{bmatrix} \tag{11}$$

$$\hat{\mathbf{S}}_{2,i} = \begin{bmatrix} \mathbf{0} \\ \mathbf{s}_{2,i} \end{bmatrix} \tag{12}$$

$$\hat{\mathbf{S}}_{3,i} = \begin{bmatrix} \mathbf{s}_{3,i} \\ \mathbf{c}_i \times \mathbf{s}_{3,i} \end{bmatrix} \tag{13}$$

$$\hat{\mathbf{S}}_{4,i} = \begin{bmatrix} \mathbf{s}_{4,i} \\ \mathbf{b}_i \times \mathbf{s}_{4,i} \end{bmatrix} \tag{14}$$

can be identified, where $\mathbf{s}_{j,i}$ represents a unit vector along the j -th joint axis of the i -th limb, $\mathbf{0}$ denotes a 3×1 zero vector, $\mathbf{b}_i = \overline{PB}$, $\mathbf{c}_i = \overline{PC} = \mathbf{b}_i - l\mathbf{1}_{i0}$, and $\mathbf{s}_{2,i} = \mathbf{s}_{3,i} = \mathbf{s}_{4,i} = \mathbf{s}_{i0}$, since the R and C joint axes are parallel to each other.

The screws that are reciprocal to all the joint screws of one limb of a 3-PCR TPM form a 2-system. Hence, two reciprocal screws of the i -th limb can be identified as two infinite-pitch wrench screws as follows.

$$\hat{\mathbf{S}}_{r,1,i} = \begin{bmatrix} \mathbf{0} \\ \mathbf{h}_{1,i} \end{bmatrix} \tag{15}$$

$$\hat{\mathbf{S}}_{r,2,i} = \begin{bmatrix} \mathbf{0} \\ \mathbf{h}_{2,i} \end{bmatrix} \tag{16}$$

where $\mathbf{h}_{1,i}$ and $\mathbf{h}_{2,i}$ are two different arbitrary vectors perpendicular to \mathbf{s}_{i0} of the i -th limb. $\hat{\mathbf{S}}_{r,1,i}$ and $\hat{\mathbf{S}}_{r,2,i}$ denote two unit couples of constraints imposed by the joints of the i -th limb, and are exerted on the mobile platform.

For simplicity, let $\mathbf{h}_{1,i}$ lie in the u - v plane and $\mathbf{h}_{2,i}$ be vertical to the u - v plane, respectively, i.e.,

$$\mathbf{h}_{1,1} = [1 \ 0 \ 0]^T$$

$$\mathbf{h}_{1,2} = \left[-\frac{1}{2} \ \frac{\sqrt{3}}{2} \ 0\right]^T$$

$$\mathbf{h}_{1,3} = \left[-\frac{1}{2} \ -\frac{\sqrt{3}}{2} \ 0\right]^T$$

$$\mathbf{h}_{2,1} = \mathbf{h}_{2,2} = \mathbf{h}_{2,3} = [0 \ 0 \ 1]$$

It is observed that the six wrench screws are linearly dependent and form a screw system of order 3, namely a 3-order wrench system of the mobile platform. Since the directions of each

C and R joint axis satisfy the conditions described earlier, i.e., they are invariable, the wrench system restricts three rotations of the mobile platform with respect to the x -, y - and z -axes of the fixed frame at any instant. Thus leads to a TPM with three translational DOF along the x -, y - and z -axes of the fixed frame.

It should be noted that the mobility of a 3-PCR TPM can also be determined by adopting other methods, such as a recent theory of degrees of freedom for complex spatial mechanisms proposed by Zhao (2004), or a group-theoretic approach recommended by Angeles (2005), etc.

3. Kinematics modeling

3.1 Inverse kinematics modeling mobility

The inverse kinematics problem solves the actuated variables from a given position of the mobile platform.

Due to the mobile platform of a 3-PCR TPM delivers only a translational motion, the position of the mobile platform with respect to the fixed frame can be described by a position vector $\mathbf{p} = [p_x \ p_y \ p_z]^T = \overline{OP}$. Besides, the position vectors of points A_i and B_i with respect to frames O and P respectively, can be written as \mathbf{a}_i and \mathbf{b}_i in the fixed frame as represented in Fig. 3. Then, a vector-loop equation can be written for i -th limb as follows:

$$l\mathbf{l}_{i0} = \mathbf{L}_i - d_i\mathbf{d}_{i0} \quad (17)$$

with

$$\mathbf{L}_i = \mathbf{p} + \mathbf{b}_i - \mathbf{a}_i + s_i\mathbf{s}_{i0} \quad (18)$$

where \mathbf{l}_{i0} is the unit vector along $\overline{C_iB_i}$, d_i represents the linear displacement of i -th actuated joint, \mathbf{d}_{i0} is the unit vector directing along rail M_iN_i , s_i denotes the stroke of i -th C joint, and \mathbf{s}_{i0} is the unit vector parallel to the axes of the C and R joints of limb i , which is denoted in Fig. 3 and can be calculated as:

$$\mathbf{s}_{i0} = [-s\varphi_i \ c\varphi_i \ 0]^T \quad (19)$$

where c stands for the cosine and s stands for the sine functions.

Substituting (18) into (17) and dot-multiplying both sides of the expression by \mathbf{s}_{i0} allows the derivation of s_i , i.e.,

$$s_i = -\mathbf{s}_{i0}^T \mathbf{p} \quad (20)$$

which lies within the range of $-s_{\max}/2 \leq s_i \leq s_{\max}/2$.

Dot-multiplying (17) with itself and rearranging the items, yields

$$d_i^2 - 2d_i\mathbf{d}_{i0}^T\mathbf{L}_i + \mathbf{L}_i^T\mathbf{L}_i - l^2 = 0 \quad (21)$$

Then, solving (21) leads to solutions for the inverse kinematics problem:

$$d_i = \mathbf{d}_{i0}^T \mathbf{L}_i \pm \sqrt{(\mathbf{d}_{i0}^T \mathbf{L}_i)^2 - \mathbf{L}_i^T \mathbf{L}_i + l^2} \tag{22}$$

We can observe that there exist two solutions for each actuated variable, hence there are totally eight possible solutions for a given mobile platform position. To enhance the stiffness of the manipulator, only the negative square root in (22) is selected to yield a solution where the three legs are inclined inward from top to bottom.

3.2 Forward kinematics modeling

Given a set of the actuated inputs, the position of the mobile platform is resolved by the forward kinematics.

From (17) and (18), we can derive that

$$l \mathbf{1}_{i0} = \mathbf{p} + s_i \mathbf{s}_{i0} - \mathbf{e}_i \tag{23}$$

where

$$\mathbf{e}_i = \mathbf{a}_i + d_i \mathbf{d}_{i0} - \mathbf{b}_i = [e_{ix} \quad e_{iy} \quad e_{iz}]^T \tag{24}$$

Dot-multiplying (23) with itself and considering (19), (20) and (24), yields

$$(p_x c^2 \varphi_i + p_y c \varphi_i s \varphi_i - e_{ix})^2 + (p_x c \varphi_i s \varphi_i + p_y s^2 \varphi_i - e_{iy})^2 + (p_z - e_{iz})^2 = l^2 \tag{25}$$

which is a system of three second-degree algebraic equations in the unknowns of p_x , p_y , and p_z .

3.2.1 Forward kinematics solutions

The analytical forward kinematics solution can be obtained by solving (25) via the Sylvester dialytic elimination method, which allows the generation of an eighth-degree polynomial in only one variable as follows.

Firstly, in order to eliminate p_y , writing (25) for $i=2$ and 3 respectively into a second-degree polynomial in p_y :

$$Ap_y^2 + Bp_y + C = 0 \tag{26}$$

$$Dp_y^2 + Ep_y + F = 0 \tag{27}$$

where $A, B, C, D, E,$ and F are all second-degree polynomials in p_x and p_z .

Taking (27) \times A - (26) \times D and (27) \times C - (26) \times F respectively, and rewriting the two equations into the matrix form as

$$\begin{bmatrix} AE - BD & AF - CD \\ CD - AF & CE - BF \end{bmatrix} \begin{bmatrix} p_y \\ 1 \end{bmatrix} = \begin{bmatrix} 0 \\ 0 \end{bmatrix} \tag{28}$$

Equation (28) represents a system of two linear equations in p_y and 1. The following equation can be obtained by equating the determinant of the coefficient matrix to zero:

$$(AE - BD)(CE - BF) + (AF - CD)^2 = 0 \tag{29}$$

Secondly, for the purpose of eliminating p_x , we write (29) in the form of

$$Lp_x^4 + Mp_x^3 + Np_x^2 + Pp_x + Q = 0 \quad (30)$$

where L, M, N, P , and Q can be shown to be second-degree polynomials in p_z .

Substituting $\varphi_1 = 0^\circ$ into (25) for $i=1$, yields

$$(p_x - e_{1x})^2 + e_{1y}^2 + (p_z - e_{1z})^2 = l^2 \quad (31)$$

which can be rewritten as:

$$Gp_x^2 + Hp_x + I = 0 \quad (32)$$

where G, H , and I are all second-degree polynomials in p_z .

Now we can eliminate the unknown p_x from (30) and (32) as follows.

Taking $(32) \times Lp_x^2 - (30) \times G$, we can obtain

$$(HL - GM)p_x^3 + (IL - GN)p_x^2 - Gpp_x - GQ = 0 \quad (33)$$

Taking $(32) \times (Lp_x^3 + Mp_x^2) - (30) \times (Gp_x + H)$, yields

$$(GN - LI)p_x^3 + (GP + HN - MI)p_x^2 + (GQ + HP)p_x + HQ = 0 \quad (34)$$

Then, multiplying (32) by p_x , we have

$$Gp_x^3 + Hp_x^2 + Ip_x = 0 \quad (35)$$

Equations (32)–(35) can be considered as four linear homogeneous equations in the four variables of p_x^3, p_x^2, p_x , and 1. The characteristic determinant is

$$\begin{vmatrix} HL - GM & IL - GN & -GP & -GQ \\ GN - LI & GP + HN - MI & GQ + HP & HQ \\ G & H & I & 0 \\ 0 & G & H & I \end{vmatrix} = 0 \quad (36)$$

Expanding (36) obtains an eight degrees of polynomial in p_z . It follows that there are at most eight solutions for p_z .

Parameter	Value	Parameter	Value
a	0.6 m	α	45°
b	0.3 m	φ_1	0°
l	0.5 m	φ_2	120°
d_{\max}	0.4 m	φ_3	240°
s_{\max}	0.2 m		

Table 1. Architectural parameters of a 3-PCR TPM

Once p_z is found, p_x and p_y can be solved by using (32) and (26) in sequence. And there are total of 32 sets of solutions for p_x , p_y , and p_z .

Although the number of solutions is considerably large, it can be shown that only one solution is feasible and the preferred solution can be determined by examining the physical constrains of the mechanism.

3.2.2 A case study

In order to illustrate the derived forward kinematics solutions, an example is introduced to identify the configurations of the manipulator.

The architectural parameters of a 3-PCR TPM are described in Table 1. Assume that the actuated values are $d_1 = 0$, $d_2 = 0$, and $d_3 = 0$. Then, the polynomial of (36) becomes

$$2.8477z^8 + 4.3284z^6 + 1.9136z^4 + 0.0714z^2 - 0.0800 = 0 \quad (37)$$

which has eight solutions for z , and the solutions for x and y can be generated from (32) and (26) in sequence, which are shown in Table 2. The imaginary values of z have no meanings, and the configurations with positive values of p_z can only be implemented by resembling the mechanism. In addition, it can be deduced that configurations 2 - 4 do not lie in the range of the manipulator workspace due to the physical constraints imposed by stroke limits of C joints and motion limits of linear actuators. Thus, only configuration 1 represents the real solution, and the unique feasible configuration is an important feature for real time control in robotic applications.

No.	z (m)	x (m)	y (m)	Configuration
1	-0.4000	0	0	1
			0.6928	2
		0.6000	0.3464	3
			1.0392	4
2	0.4000	—	—	—
3	0.7483i	—	—	—
4	-0.7483i	—	—	—
5	0.7483i	—	—	—
6	-0.7483i	—	—	—
7	0.7483i	—	—	—
8	-0.7483i	—	—	—

Table 2. Forward kinematics solutions obtained via analytical method

4. Velocity analysis

Substituting (18) into (17) and differentiating the expression with respect to time, leads to

$$\dot{d}_i \mathbf{d}_{i0} = \dot{\mathbf{x}} - l \omega_i \times \mathbf{l}_{i0} + \dot{s} \mathbf{s}_{i0} \quad (38)$$

where ω_i is the angular velocity of i -th limb with respect to the fixed frame, and $\dot{\mathbf{x}} = [\dot{p}_x \ \dot{p}_y \ \dot{p}_z]^T$ is the linear velocity of the mobile platform.

Dot-multiplying both sides of (38) by \mathbf{l}_{i0} , gives

$$\mathbf{l}_{i0}^T \mathbf{d}_{i0} \dot{d}_i = \mathbf{l}_{i0}^T \dot{\mathbf{x}} \quad (39)$$

Writing (39) three times, once for each $i=1, 2$, and 3 , yields three scalar equations which can be written in the matrix form:

$$\mathbf{J}_q \dot{\mathbf{q}} = \mathbf{J}_x \dot{\mathbf{x}} \quad (40)$$

where the matrices

$$\mathbf{J}_q = \begin{bmatrix} \mathbf{l}_{10}^T \mathbf{d}_{10} & 0 & 0 \\ 0 & \mathbf{l}_{20}^T \mathbf{d}_{20} & 0 \\ 0 & 0 & \mathbf{l}_{30}^T \mathbf{d}_{30} \end{bmatrix}, \quad \mathbf{J}_x = \begin{bmatrix} \mathbf{l}_{10}^T \\ \mathbf{l}_{20}^T \\ \mathbf{l}_{30}^T \end{bmatrix} \quad (41)$$

and $\dot{\mathbf{q}} = [\dot{d}_1 \ \dot{d}_2 \ \dot{d}_3]^T$ is the vector of actuated joint rates.

When the manipulator is away from singularities, the following velocity equations can be derived from (41).

$$\dot{\mathbf{q}} = \mathbf{J} \dot{\mathbf{x}} \quad (42)$$

where

$$\mathbf{J} = \mathbf{J}_q^{-1} \mathbf{J}_x \quad (43)$$

is the 3×3 Jacobian matrix of a 3-PCR TPM, which relates the output velocities to the actuated joint rates.

5. Singularity identification and elimination

For a parallel manipulator, the singularity configuration results in a loss of controllability and degradation of natural stiffness of the manipulator. Therefore, the analysis of parallel manipulator singularities, which is necessary for both the design and control purposes, has drawn considerable attentions (Di Gregorio & Parenti-Castelli, 1999; Zlatanov et al., 2002).

5.1 Singular configurations identification

Four kinds of singularities can be identified for a 3-PCR TPM as follows.

1) The first kind of singularity, which is also called the inverse kinematics singularity, occurs when \mathbf{J}_q is not of full rank and \mathbf{J}_x is invertible, i.e., $\det(\mathbf{J}_q) = 0$ and $\det(\mathbf{J}_x) \neq 0$.

We can see that this is the case when $\mathbf{l}_{i0}^T \mathbf{d}_{i0} = 0$ for $i=1, 2$, or 3 , i.e., the directions of one or more of legs are perpendicular to the axial directions of the corresponding actuated joints. In this case, the mobile platform loses one or more DOF, which always occurs on the boundary of the workspace and can be avoided by restricting the motional range of the actuators.

2) The second kind of singularity also called the direct kinematics singularity occurs when \mathbf{J}_x is not of full rank while \mathbf{J}_q is invertible, i.e., $\det(\mathbf{J}_q) \neq 0$ and $\det(\mathbf{J}_x) = 0$.

We can deduce that it is the case when \mathbf{l}_{i0} for $i=1, 2,$ and 3 become linearly dependent. Physically, this type of singularity occurs when two or three of legs are parallel to one another, or the three legs lie in a common plane. Under such case, the manipulator gains one or more DOF even when all actuators are locked, which could be avoided by proper architecture design of the manipulator.

3) The third kind of singularity occurs when both \mathbf{J}_q and \mathbf{J}_x become simultaneously not invertible, i.e., $\det(\mathbf{J}_q) = 0$ and $\det(\mathbf{J}_x) = 0$. Under a singularity of this type, the mobile platform can undergo finite motions even when the actuators are locked, or equivalently, it cannot resist to forces or moments in one or more directions even if all actuators are locked. And a finite motion of the actuators gives no motion of the mobile platform.

4) Besides the three types of singularities, the rotational singularity for a TPM may occur when the mobile platform of a TPM can rotate instantaneously (Di Gregorio & Parenti-Castelli, 1999). This concept has been generalized to the constraint singularity of limited-DOF parallel manipulators (Zlatanov et al., 2002). And this type of singularity arises when the kinematic chains of a limited-DOF parallel manipulator cannot constrain the mobile platform to the planned motion any more. As far as a 3-PCR TPM is concerned, it is shown based on screw theory in Section 2 that the mobile platform cannot rotate at any instant, thus there is no rotational singularity for the 3-PCR TPM.

5.2 Mechanism design to eliminate singularities

The singular configurations can be eliminated by the approach of mechanism design as follows.

1) Elimination of the direct kinematics singularities: According to the aforementioned analysis, three cases can be classified for the direct kinematics singularity.

Case I- two legs are parallel to each other. Assume that \mathbf{l}_{10} is parallel to \mathbf{l}_{20} . For simplicity, let the 3-PCR TPM possess a symmetric architecture. It can be deduced that \mathbf{l}_{10} and \mathbf{l}_{20} are perpendicular to the base plane. Generating \mathbf{s}_{10} and \mathbf{p} , and substituting them into (20) for $i=1$, allows the generation of $s_1 = \sqrt{3}(a - b - d_1c\alpha)$, where $d_1 = d_2$. With the consideration of (2), the maximum stroke of C joints should be designed as

$$s_{max} < 2\sqrt{3}(a - b - \frac{d_{max}}{2}c\alpha) \tag{44}$$

in order to eliminate this kind of singular configurations.

Case II - the three legs are parallel to one another. Under such case, it is seen that the three vectors \mathbf{l}_{i0} , for $i=1, 2,$ and 3 , are all perpendicular to the base plane. In addition, $d_1 = d_2 = d_3$ and $b = a - d_1c\alpha$. To eliminate this singularity, the maximum stroke of linear actuators should be designed as

$$d_{max} < 2d_1 = \frac{2(a - b)}{c\alpha}, \text{ if } \alpha \neq 90^\circ \tag{45}$$

Case III - the three legs lie in a common plane. In this situation, the three vectors \mathbf{I}_{10} lie in a plane parallel to the base plane. It can be deduced that $d_1 = d_2 = d_3$ and $b+l = a \pm d_1 c \alpha$. To eliminate this singularity, the maximum stroke of linear actuators should be designed as

$$d_{max} < 2d_1 = \frac{2a-b-l}{c\alpha}, \quad \text{if } \alpha \neq 90^\circ \quad (46)$$

2) Elimination of the combined singularities: From above discussions, we can see that the combined singularity occurs in the cases of $\alpha = 0^\circ$ with $d_1 = d_2 = d_3 = a - b$, or $\alpha = 90^\circ$ with $a = b + l$. Thus, we can eliminate this type of singularities by the design of

$$d_{max} < 2(a - b), \quad \text{if } \alpha = 0^\circ \quad (47)$$

$$a < b + l, \quad \text{if } \alpha = 90^\circ \quad (48)$$

Therefore, in a real machine design, (44)–(48) should be satisfied at the same time so as to eliminate all of the singular configurations from the workspace of a 3-PCR TPM.

6. Isotropic configurations

An isotropic manipulator is a manipulator with the Jacobian matrix having a condition number equal to 1 in at least one of its configurations. In isotropic configurations, the manipulator performs very well with regard to the force and velocity transmission. As for a 3-PCR TPM in isotropic configurations, the Jacobian matrix \mathbf{J} should satisfy:

$$\mathbf{J}\mathbf{J}^T = \sigma \mathbf{I}_{3 \times 3} \quad (49)$$

where $\mathbf{I}_{3 \times 3}$ is a 3×3 identity matrix. Under such a case, in view of (43), the following conditions must hold:

$$\sigma = \mathbf{t}_i^T \mathbf{t}_i = 1 \quad (50)$$

$$\mathbf{t}_i^T \mathbf{t}_j = 0 \quad \text{for } i \neq j \quad (51)$$

for $i, j=1, 2$, and 3 .

From (51), we can see that the three vectors \mathbf{t}_i are perpendicular to one another. Writing (51) three times, once for each $i=1, 2$, and 3 , respectively, results in three equations in the unknowns of p_x , p_y , and p_z . Solving them allows the generation of isotropic configurations. Given the symmetric architecture of a 3-PCR TPM, the isotropic configurations, which lie along the z -axis, can be derived by

$$\mathbf{p} = [0 \quad 0 \quad -d\alpha \pm \frac{\sqrt{2}}{2}(a - b - dc\alpha)]^T \quad (52)$$

where $d = d_1 = d_2 = d_3$. Only the negative sign is taken into consideration since we are interested only in the point below the actuators.

Moreover, under such a case, the relationship between architectural parameters can be derived through a careful analysis, i.e.,

$$l = \frac{\sqrt{6}}{2}(a - b - dc\alpha) \tag{53}$$

Deriving d from (53) and in view of (1), allows the generation of

$$\begin{cases} -\frac{d_{max}}{2} \leq \frac{a - b - \frac{\sqrt{6}}{3}l}{c\alpha} \leq \frac{d_{max}}{2} & \text{if } \alpha \neq 90^\circ \\ a - b = \frac{\sqrt{6}}{3}l & \text{if } \alpha = 90^\circ \end{cases} \tag{54}$$

which are the isotropy conditions resulting in an isotropic 3-PCR TPM.

7. Workspace determination

As is well known, with comparison to their serial counterparts, parallel manipulators have relatively small workspace. Thus the workspace of a parallel manipulator is one of the most important aspects to reflect its working ability, and it is necessary to analyze the shape and volume of the workspace for enhancing applications of parallel manipulators. The reachable workspace of a 3-PCR TPM presented here is defined as the space that can be reached by the reference point P .

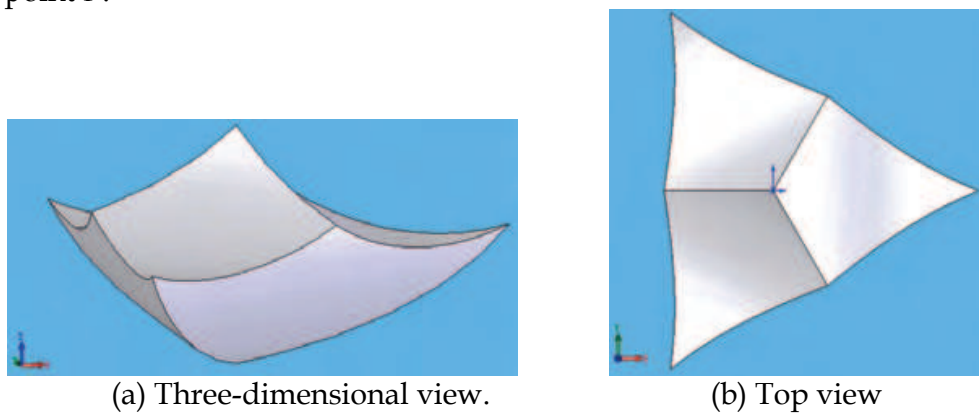


Fig. 5. Workspace of a 3-PCR TPM without constraints on C joints.

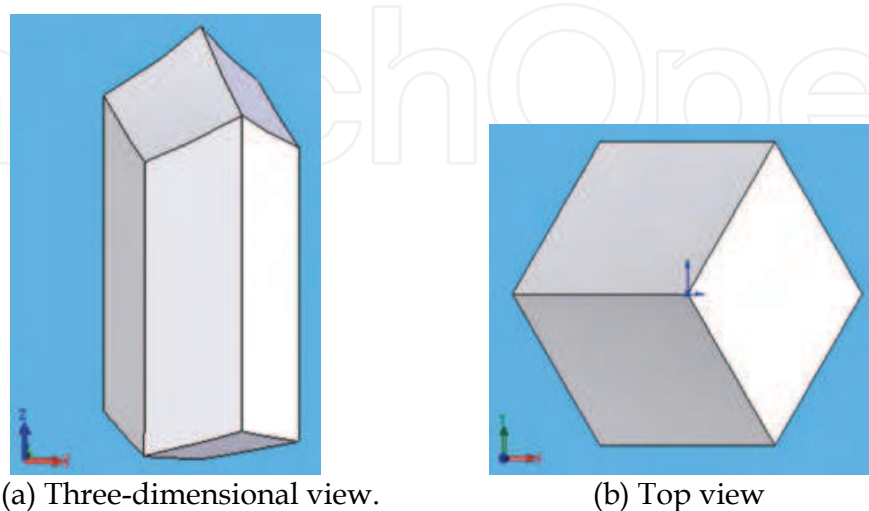


Fig. 6. Workspace of a 3-PCR TPM with constraints on C joints.

7.1 Analytical method

The TPM workspace can be generated by considering (25), which denotes the workspace of the i -th limb ($i=1, 2, 3$). With the substitution of constant vectors, (25) can be expanded into the following forms:

$$[p_x + d_1 c\alpha - (a - b)]^2 + (p_z + d_1 s\alpha)^2 = l^2 \quad (55)$$

$$\left\{ \frac{1}{4}(p_x - \sqrt{3}p_y) - \frac{1}{2}[d_2 c\alpha - (a - b)] \right\}^2 + \left\{ \frac{-\sqrt{3}}{4}(p_x - \sqrt{3}p_y) + \frac{\sqrt{3}}{2}[d_2 c\alpha - (a - b)] \right\}^2 + (p_z + d_2 s\alpha)^2 = l^2 \quad (56)$$

$$\left\{ \frac{1}{4}(p_x + p_y) - \frac{1}{2}[d_3 c\alpha - (a - b)] \right\}^2 + \left\{ \frac{\sqrt{3}}{4}(p_x + p_y) - \frac{\sqrt{3}}{2}[d_3 c\alpha - (a - b)] \right\}^2 + (p_z + d_3 s\alpha)^2 = l^2 \quad (57)$$

As d_i varying within the range of $-d_{\max}/2 \leq d_i \leq d_{\max}/2$, each one of the above equations denotes a set of cylinders with the radii of l . The manipulator workspace can be derived geometrically by the intersection of the three limbs' workspace.

As a case study, for a 3-PCR TPM with kinematic parameters described in Table 1, the workspace without the constraints on the stroke of passive C joints is illustrated in Fig. 5. With the consideration of the stroke limits of C joints, the whole reachable workspace of the CPM is depicted in Fig. 6. It can be seen that the C joints bring six boundary planes to the workspace, and lead to a reachable workspace with a hexagon shape on cross section.

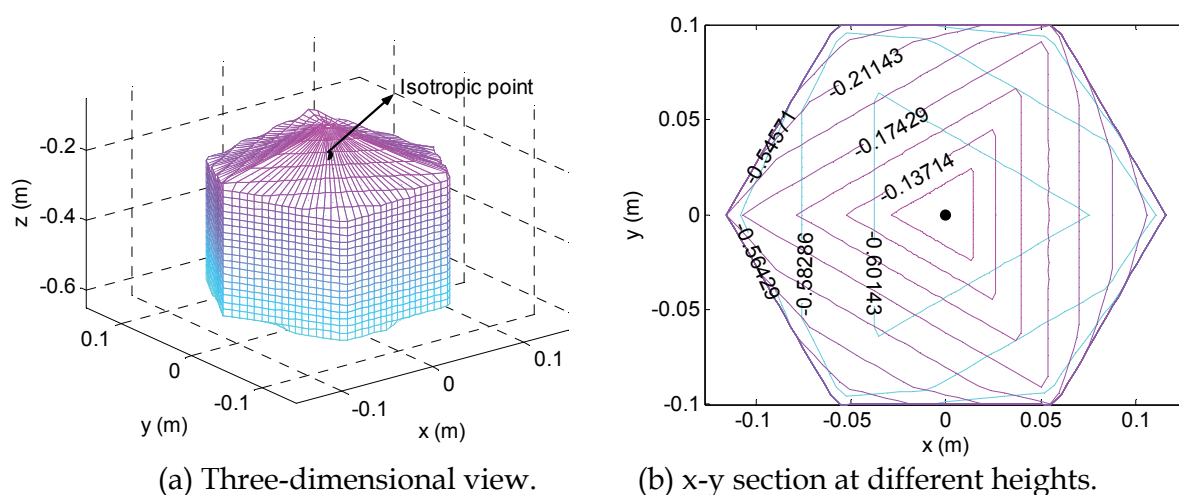


Fig. 7. Reachable workspace of a 3-PCR TPM via a numerical method.

7.2 Numerical approach

An observation of the TPM workspace obtained via the analytical approach reveals that there exists no void within the workspace, i.e., the cross section of the workspace is consecutive at every height. Then a numerical search method can be adopted in cylindrical

coordinates by slicing the workspace into a series of sub-workspace (Li & Xu, 2007), and the boundary of each sub-workspace is successively determined based on the inverse kinematics solutions along with the physical constraints taken into consideration. The total workspace volume is approximately calculated as the sum of these sub-workspaces. The adopted numerical approach can also facilitate the dexterity analysis of the manipulator discussed later.

For a 3-PCR TPM as described in Table 1, it has been designed so as to eliminate all of the singular configurations from the workspace and also to generate an isotropic configuration. Calculating d from (53) and substituting it into (52), allows the derivation of the isotropic configuration, i.e., $\mathbf{p} = [0 \ 0 \ -0.1804]^T$.

The workspace of the manipulator is generated numerically by a developed MATLAB program and illustrated in Fig. 7, where the isotropic point is also indicated. It is observed that the reachable workspace is 120 degree-symmetrical about the three motion directions of actuators from overlook, and can be divided into the upper, middle, and lower parts. In the minor upper and lower parts of the workspace, the cross sections have a triangular shape. While in the definitive major middle range of the workspace, most of the applications will be performed, it is of interest to notice that the proposed manipulator has a uniform workspace without variation of the cross sectional area which takes on the shape of a hexagon.

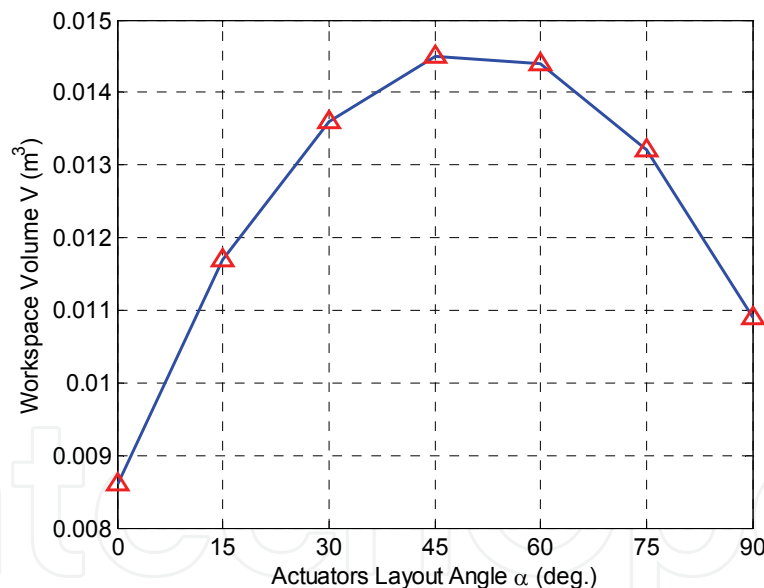


Fig. 8. Workspace volume versus actuators layout angle.

Additionally, it is necessary to identify the impact on the workspace with the variation of architecture parameters. For the aforementioned 3-PCR TPM, with the varying of actuators layout angle (α), the simulation results of the workspace volumes are shown in Fig. 8. We can observe that the maximum workspace volume occurs when α is around 45° . It can be shown that there exist no singular configurations along with the varying of α , but the manipulator possesses no isotropic configurations if $\alpha > 57.2^\circ$. The simulation results reveal the roles of conditions expressed by (44) – (48) and (54) in designing a 3-PCR TPM.

8. Dexterity analysis

Dexterity is an important issue for design, trajectory planning, and control of manipulators, and has emerged as a measure for manipulator kinematic performance. The dexterity of a manipulator can be thought as the ability of the manipulator to arbitrarily change its position and orientation, or apply forces and torques in arbitrary directions. In this section, we focus on discovering the dexterity characteristics of a 3-PCR TPM in a local sense and global sense, respectively.

8.1 Dexterity indices

In the literature, different indices of manipulator dexterity have been introduced. One of the frequently used indices is called kinematic manipulability expressed by the square root of the determinant of $\mathbf{J}\mathbf{J}^T$,

$$\omega = \sqrt{\det(\mathbf{J}\mathbf{J}^T)} \quad (58)$$

Since the Jacobian matrix (\mathbf{J}) is configuration dependent, kinematic manipulability is a local performance measure, which also gives an indication of how close the manipulator is to the singularity. For instance, $\omega = 0$ means a singular configuration, and therefore we wish to maximize the manipulability index to avoid singularities.

Another usually used index is the condition number of Jacobian matrix. As a measure of dexterity, the condition number ranges in value from one (isotropy) to infinity (singularity) and thus measures the degree of ill-conditioning of the Jacobian matrix, i.e., nearness of the singularity, and it is also a local measure dependent solely on the configuration, based on which a global dexterity index (GDI) is proposed by Gosselin & Angeles (1991) as follows:

$$GDI = \frac{\int_V (\frac{1}{\kappa}) dV}{V} \quad (59)$$

where V is the total workspace volume, and κ denotes the condition number of the Jacobian and can be defined as $\kappa = \|\mathbf{J}\| \|\mathbf{J}^{-1}\|$, with $\|\bullet\|$ denoting the 2-norm of the matrix. Moreover, the GDI represents the uniformity of dexterity over the entire workspace other than the dexterity at certain configuration, and can give a measure of kinematic performance independent of the different workspace volumes of the design candidates since it is normalized by the workspace size.

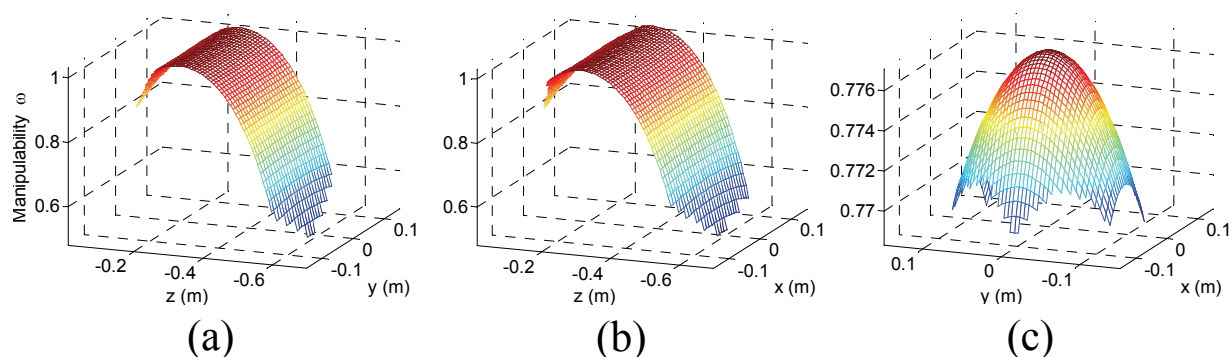


Fig. 9. Manipulability distribution of a 3-PCR TPM in three planes of (a) $x = 0$, (b) $y = 0$, and (c) $z = -0.5$ m.

8.2 Case studies

8.2.1 Kinematic manipulability

Regarding a 3-PCR TPM, since it is a nonredundant manipulator, the manipulability measure ω is reduced to

$$\omega = |det(\mathbf{J})| \tag{60}$$

With actuators layout angle $\alpha = 30^\circ$ and other parameters as described in Table 1, the manipulability of a 3-PCR TPM in the planes of $x=0$, $y=0$, and $z=-0.5$ is shown in Fig. 9. It can be observed from Figs. 9(a) and 9(b) that in y - z and x - z planes, manipulability is maximal when the center point of the mobile platform lies in the z -axis and at the height of the isotropic point, and decreases when the mobile platform is far from the z -axis and away from the isotropic point. From Fig. 9(c), it is seen that in a plane at certain height, manipulability is maximal when the mobile platform lies along the z -axis, and decreases in case of the manipulator approaching to its workspace boundary.

8.2.2 Global dexterity index (GDI)

Since there are no closed-form solutions for (59), the integral of the dexterity can be calculated numerically by an approximate discrete sum

$$GDI \approx \frac{1}{N_w} \sum_{w \in I} \frac{1}{\kappa} \tag{61}$$

where w is one of N_w points uniformly distributed over the entire workspace of the manipulator.

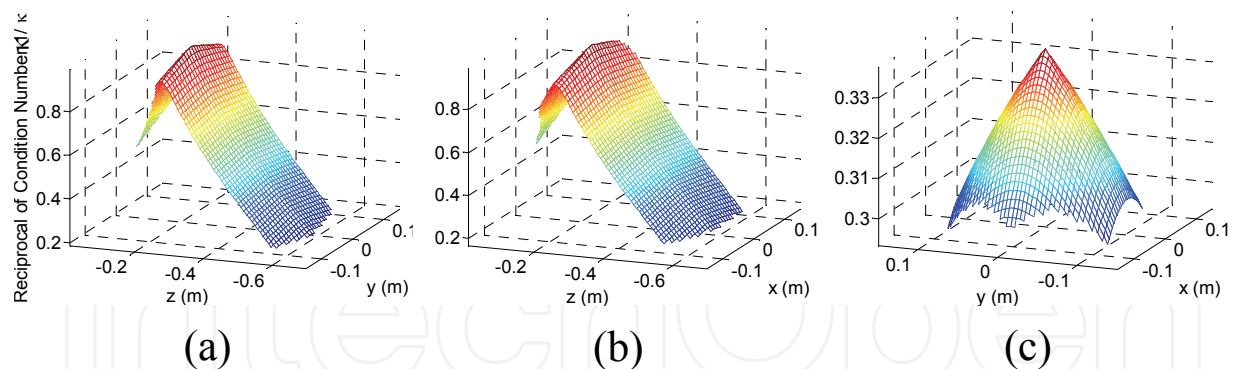


Fig. 10. Distribution of reciprocal of the condition number for a 3-PCR TPM in three planes of (a) $x = 0$, (b) $y = 0$, and (c) $z = -0.5$ m.

Figures from 10(a) to 10(c) respectively illustrate the distribution of the reciprocal of Jacobian matrix condition number in three planes of $x = 0$, $y = 0$, and $z = -0.5$ m for a 3-PCR TPM with $\alpha = 30^\circ$ and other parameters depicted in Table 1. It is observed that the figures show the similar yet sharper tendencies of changes than those in Fig. 8. With the changing of layout angle of actuators, we can calculate the GDI of the 3-PCR TPM over the entire workspace, and the simulation results are shown in Fig. 11. We can observe that the maximum value of GDI occurs when $\alpha = 0^\circ$, and decreases along with the increasing of

layout angle of actuators. However, with $\alpha = 0^\circ$ it is seen from Fig. 8 that the workspace volume is relatively small. Since the selection of a manipulator depends heavily on the task to be performed, different objectives should be taken into account when the actuators layout angle of a 3-PCR TPM is designed, or alternatively, several required performance indices may be considered simultaneously.

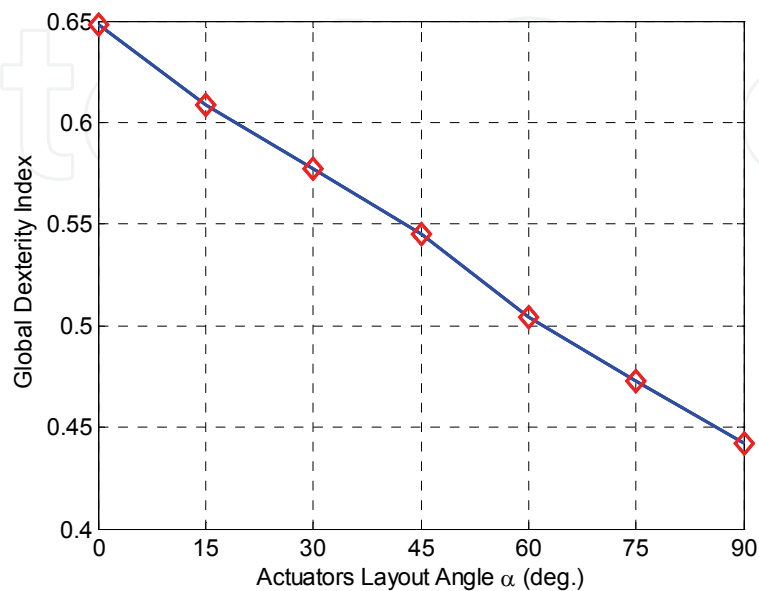


Fig. 11. Global dexterity index versus actuators layout angle.

9. Application of a 3-PCR TPM as a CPR medical robot

9.1 Requirements of CPR

It is known that in case of a patient being in cardiac arrest, cardiopulmonary resuscitation (CPR) must be applied in both rescue breathing (mouth-to-mouth resuscitation) and chest compressions. Generally, the compression frequency for an adult is at the rate of about 100 times per minute with the depth of 4 to 5 centimeters using two hands, and the CPR is usually performed with the compression-to-ventilation ratio of 15 compressions to 2 breaths so as to maintain oxygenated blood flowing to vital organs and to prevent anoxic tissue damage during cardiac arrest (Bankman et al, 1990). Without oxygen, permanent brain damage or death can occur in less than 10 minutes. Thus for a large number of patients who undergo unexpected cardiac arrest, the only hope of survival is timely applying CPR. However, some patients in cardiac arrest may be also infected with other indeterminate diseases, and it is very dangerous for a doctor to apply CPR to them directly. For example, before the severe acute respiratory syndrome (SARS) was first recognized as a global threat in 2003, in many hospitals such kinds of patients were rescued as usual, and some doctors who had performed CPR to such patients were finally infected with the SARS corona virus unfortunately. In addition, chest compressions consume a lot of energies from doctors. For instance, sometimes it needs ten doctors to work two hours to perform chest compressions to rescue a patient in a Beijing hospital of China, because the energy spent on chest compression is consumed greatly so as to one doctor could not insist on doing the job without any rest. Therefore a medical robot applicable to chest compressions is urgently

required. In view of this practical requirement, we will propose the conceptual design of a medical parallel robot to assist in CPR operation, and wish the robot can perform this job well in stead of doctors.

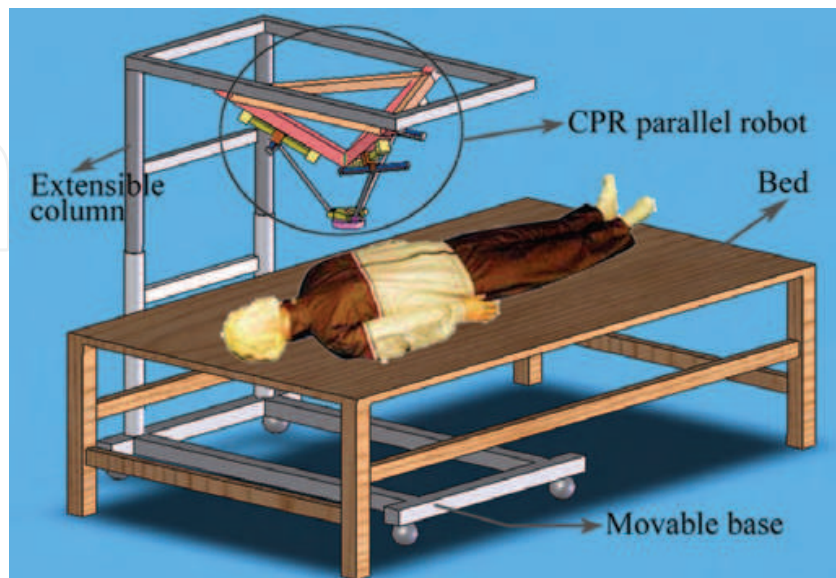


Fig. 12. Conceptual design of a CPR medical robot system.

9.2 Conceptual design of a CPR robot system

A conceptual design of the medical robot system is illustrated in Fig. 12. As shown in the figure, the patient is placed on a bed beside a CPR robot which is mounted on a separated movable base via two supporting columns and is placed above the chest of the patient. The movable base can be moved anywhere on the ground and the supporting columns are extensible in the vertical direction. Thus, the robot can be positioned well by hand so that the chest compressions may start as soon as possible, which also allows a doctor to easily take the robot away from the patient in case of any erroneous operation. Moreover, the CPR robot is located on one side of the patient, thereby providing a free space for a rescuer to access to the patient on the other side.

In view of the high stiffness and high accuracy properties, parallel mechanisms are employed to design such a manipulator applicable to chest compressions in CPR. This idea is motivated from the reason why the rescuer uses two hands instead of only one hand to perform the action of chest compressions. In the process of performing chest compressions, the two arms of the rescuer construct similarly a parallel mechanism. The main disadvantage of parallel robots is their relatively limited workspace range. Fortunately, by a proper design, a parallel robot is able to satisfy the workspace requirement with a height of 4–5 centimeters for the CPR operation.

In the next step, it comes with the problem of how to select a particular parallel robot for the application of CPR since nowadays there exist a lot of parallel robots providing various types of output motions. An observation of the chest compressions in manual CPR reveals that the most useful motion adopted in such an application is the back and forth translation in a direction vertical to the patient's chest, whereas the rotational motions are almost

useless. Thus, parallel robots with a total of six DOF are not necessary required here. Besides, a 6-DOF parallel robot usually possesses some disadvantages in terms of complicated forward kinematics problems and highly-coupled translation and rotation motions, etc., which complicate the control problem of such kind of robot. Hence, TPMs with only three translational DOF in space are sufficient to be employed in CPR operation. Because in addition to a translation vertical to the chest of the patient, a 3-DOF TPM can also provide translations in any other directions, which enables the adjustment of the manipulator's moving platform to a suitable position to perform chest compression tasks. At this point, TPMs with less than three DOF are not adopted here.

As far as a 3-DOF TPM is concerned, it can be designed as various architectures with different mechanical joints. Here, we adopt the type of TPMs whose actuators are mounted on the base, since this property enables large powerful actuators to drive relatively small structures, facilitating the design of the manipulator with faster, stiffer, and stronger characteristics. In addition, from the economic point of view, the simpler of the architecture of a TPM is, the lower cost it will be spent. In view of the complexity of the TPM topology including the number of mechanical joints and links and their manufacture procedures, the proposed 3-PCR TPM is chosen to develop a CPR medical robot. It should be noted that, theoretically, other architectures such as the Delta or linear Delta like TPMs can be employed in a CPR robot system as well.

10. Structure variations of a 3-PCR TPM

The three guide ways of a 3-PCR TPM can be arranged in other schemes to generate various kinds of TPMs. For example, a 3-PCR TPM with an orthogonal structure is shown in Fig. 13. The orthogonal 3-PCR TPM has a cubic shape workspace as illustrated in Fig. 14. Moreover, the TPM has a partially decoupled translational motion. Hence, the orthogonal 3-PCR TPM has a potentially wider application than the former one, especially in micro/nano scale manipulation fields.

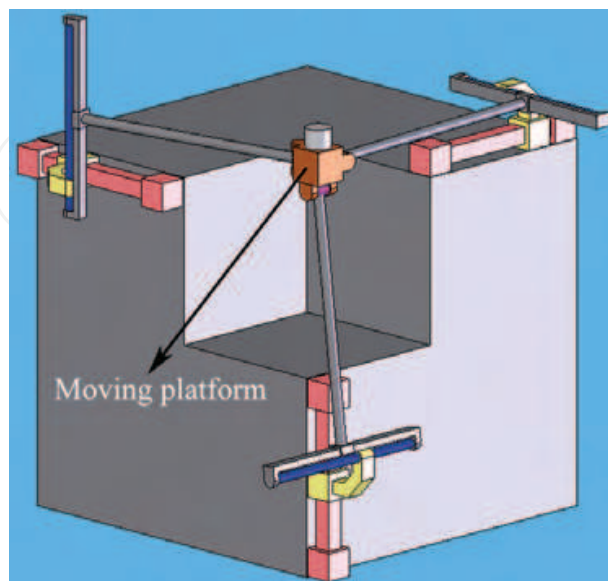


Fig. 13. A 3-PCR TPM with orthogonal guide ways.

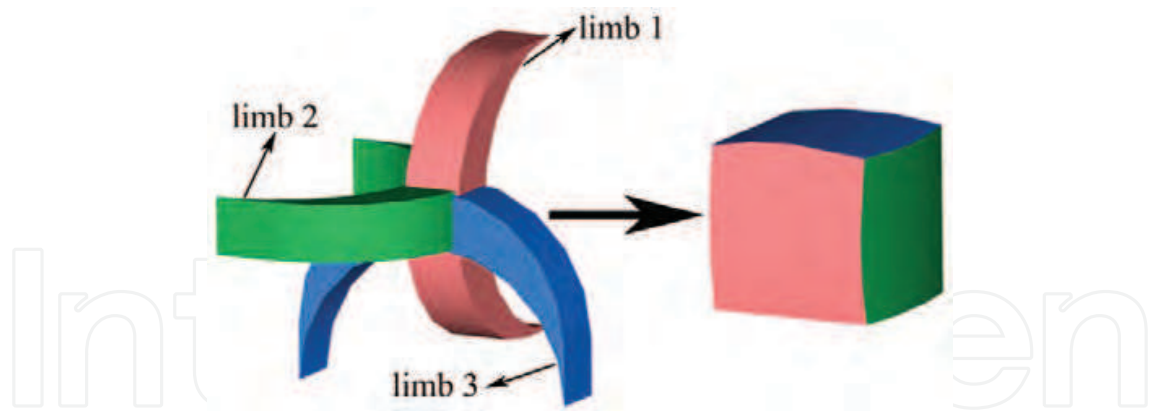


Fig. 14. Workspace determination for an orthogonal 3-PCR TPM.

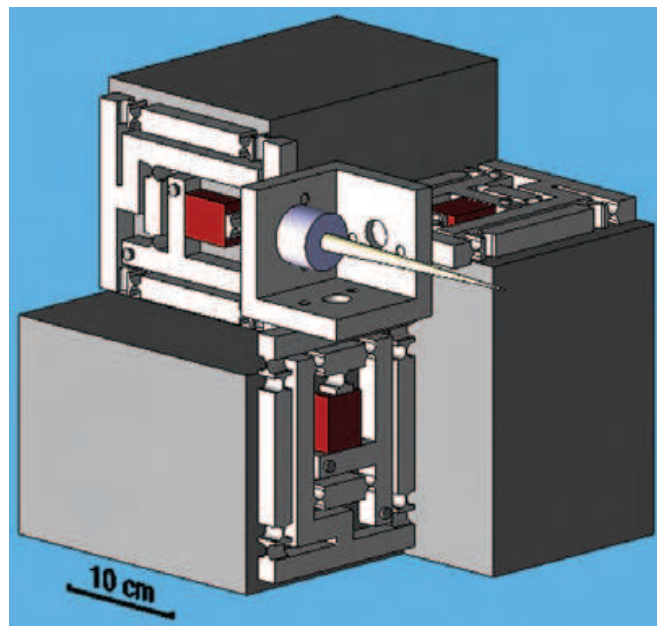


Fig. 15. A micro 3-PCR TPM designed for micro/nano manipulation.

For instance, a 3-PCR parallel micro-manipulator designed for ultrahigh precision manipulation is shown in Fig. 15. The flexure hinges are adopted due to their excellent characteristics over traditional joints in terms of vacuum compatibility, no backlash property, no nonlinear friction, and simple structure and easy to manufacture, etc. Besides, in view of greater actuation force, higher stiffness, and faster response characteristics of piezoelectric actuators (PZTs), they are selected as linear actuators of the micro-manipulator. Thanks to a high resolution motion, it is expected that the piezo-driven flexure hinge-based parallel micro-manipulator can find its way into micro/nano scale manipulation.

11. Conclusion

In this chapter, a new class of translational parallel manipulator with 3-PCR architecture has been proposed. It has been shown that such a mechanism can act as an overconstrained 3-DOF translational manipulator with some certain assembling conditions satisfied. Since the

proposed 3-PCR TPMs possess smaller mobile platform size than the corresponding 3-PRC ones, they have wider application such as the rapid pick-and-place operation over a limited space, etc.

The inverse and forward kinematics, velocity equations, and singular and isotropic configurations have been derived. And the singularities have been eliminated from the manipulator workspace by a proper mechanism design. The reachable workspace is generated by an analytical as well as a numerical way, and the dexterity performances of the TPM have been investigated in detail. As a new application, the designed 3-PCR TPM has been adopted as a medical robot to assist in CPR. Furthermore, another 3-PCR TPM with orthogonally arranged guide ways has been presented as well, which possesses a partially decoupled motion within a cubic shape workspace and its application in micro/nano scale ultrahigh precision manipulation has been exploited by virtue of flexure hinge-based joints and piezoelectric actuation. Several virtual prototypes of the 3-PCR TPM are graphically shown for the purpose of illustrating their different applications.

The results presented in the chapter will be valuable for both the design and development of a new class of TPMs for various applications.

12. References

- Angeles, J. (2005). The degree of freedom of parallel robot: A group-theoretic approach. *Proceedings of IEEE International Conference on Robotics and Automation*, pp. 1005-1012, Barcelona, Spain, Apr. 2005.
- Bankman, I. N.; Gruben, K. G.; Halperin, H. R.; Popel, A. S.; Guerci, A. D. & Tsitlik, J. E. (1990). Identification of dynamic mechanical parameters of the human chest during manual cardiopulmonary resuscitation, *IEEE Transactions on Biomedical Engineering*, Vol. 37, No. 2, pp. 211-217, Feb. 1990, ISSN 0018-9294.
- Callegari, M. & Tarantini, M. (2003). Kinematic analysis of a novel translational platform, *ASME Journal of Mechanical Design*, Vol. 125, No. 2, pp. 308-315, June 2003, ISSN 1050-0472.
- Chablat, D. & Wenger, P. (2003). Architecture optimization of a 3-DOF translational parallel mechanism for machining applications, the Orthoglide, *IEEE Transactions on Robotics and Automation*, Vol. 19, No. 3, pp. 403-410, June 2003, ISSN 1042-296X.
- Clavel, R. (1988). DELTA, a fast robot with parallel geometry, *Proceedings of 18th International Symposium on Industrial Robots*, pp. 91-100, Lausanne, Switzerland, 1988.
- Di Gregorio, R. & Parenti-Castelli, V. (1999). Mobility analysis of the 3-UPU parallel mechanism assembled for a pure translational motion, *Proceedings of IEEE/ASME International Conference on Advanced Intelligent Mechatronics*, pp. 520-525, Atlanta, Georgia, USA, Sep. 1999.
- Gosselin, C. & Angeles, J. (1991). A global performance index for the kinematic optimization of robotic manipulators, *ASME Journal of Mechanical Design*, Vol. 113, No. 3, pp. 220-226, Sep. 1991, ISSN 1050-0472.
- Hunt, K. H. (1990). *Kinematic Geometry of Mechanisms*, Oxford University Press, ISBN 0198562330, New York.

- Kim, D. & Chung, W. K. (2003). Kinematic condition analysis of three-DOF pure translational parallel manipulators, *ASME Journal of Mechanical Design*, Vol. 125, No. 2, pp. 323–331, June 2003, ISSN 1050-0472.
- Kim, H. S. & Tsai, L.W. (2003). Design optimization of a Cartesian parallel manipulator, *ASME Journal of Mechanical Design*, Vol. 125, No. 1, pp. 43–51, Mar. 2003, ISSN 1050-0472.
- Kong, X. & Gosselin, C. M. (2002). Kinematics and singularity analysis of a novel type of 3-CRR 3-DOF translational parallel manipulator, *International Journal of Robotics Research*, Vol. 21, No. 9, pp. 791–798, Sep. 2002, ISSN 0278-3649.
- Kong, X. & Gosselin, C. M. (2004). Type synthesis of 3-DOF translational parallel manipulators based on screw theory, *ASME Journal of Mechanical Design*, Vol. 126, No. 1, pp. 83–92, Mar. 2004, ISSN 1050-0472.
- Li, Y. & Xu, Q. (2005). Dynamic analysis of a modified DELTA parallel robot for cardiopulmonary resuscitation, *Proceedings of IEEE/RSJ International Conference on Intelligent Robots and Systems*, pp. 3371–3376, Edmonton, Alberta, Canada, Aug. 2005.
- Li, Y. & Xu, Q. (2006). Kinematic analysis and design of a new 3-DOF translational parallel manipulator, *ASME Journal of Mechanical Design*, Vol. 128, No. 4, pp. 729–737, Jul. 2006, ISSN 1050-0472.
- Li, Y. & Xu, Q. (2007). Kinematic analysis of a 3-PRS parallel manipulator, *Robotics and Computer-Integrated Manufacturing*, Vol. 23, No. 4, pp. 395–408, Aug. 2007, ISSN 0736-5845.
- Merlet, J.-P. (2000). *Parallel Robots*, Kluwer Academic Publishers, ISBN 1402003854, London.
- Tsai, L. W.; Walsh, G. C. & Stamper, R. E. (1996). Kinematics of a novel three dof translational platform, *Proceedings of IEEE International Conference on Robotics and Automation*, pp. 3446–3451, Minneapolis, Minnesota, USA, Apr. 1996.
- Tsai, L. W. & Joshi, S. (2002). Kinematics analysis of 3-DOF position mechanisms for use in hybrid kinematic machines, *ASME Journal of Mechanical Design*, Vol. 124, No. 2, pp. 245–253, Jun. 2002, ISSN 1050-0472.
- Xu, Q. & Li, Y. (2007). Design and analysis of a new singularity-free three-prismatic-revolute-cylindrical translational parallel manipulator, *Proceedings of The Institution of Mechanical Engineers Part C-Journal of Mechanical Engineering Science*, Vol. 221, No. 5, pp. 565–577, May 2007, ISSN 0954-4062.
- Zhao, J.-S.; Zhou, K. & Feng, Z.-J. (2004). A theory of degrees of freedom for mechanisms. *Mechanism and Machine Theory*, Vol. 39, No. 6, pp. 621–643, June 2004, ISSN 0094-114X.
- Zhao, T. S. & Huang, Z. (2000). A novel three-DOF translational platform mechanism and its kinematics, *Proceedings of ASME Design Engineering Technical Conferences & Computers and Information in Engineering Conference*, paper number DETC2000/MECH-14101, Baltimore, Maryland, USA, Sep. 2000.

Zlatanov, D.; Bonev, I. A. & Gosselin, C. M. (2002). Constraint singularities of parallel mechanisms, *Proceedings of IEEE International Conference on Robotics and Automation*, pp. 496-502, Washington D.C., USA, May 2002.

IntechOpen

IntechOpen



Parallel Manipulators, New Developments

Edited by Jee-Hwan Ryu

ISBN 978-3-902613-20-2

Hard cover, 498 pages

Publisher I-Tech Education and Publishing

Published online 01, April, 2008

Published in print edition April, 2008

Parallel manipulators are characterized as having closed-loop kinematic chains. Compared to serial manipulators, which have open-ended structure, parallel manipulators have many advantages in terms of accuracy, rigidity and ability to manipulate heavy loads. Therefore, they have been getting many attentions in astronomy to flight simulators and especially in machine-tool industries. The aim of this book is to provide an overview of the state-of-art, to present new ideas, original results and practical experiences in parallel manipulators. This book mainly introduces advanced kinematic and dynamic analysis methods and cutting edge control technologies for parallel manipulators. Even though this book only contains several samples of research activities on parallel manipulators, I believe this book can give an idea to the reader about what has been done in the field recently, and what kind of open problems are in this area.

How to reference

In order to correctly reference this scholarly work, feel free to copy and paste the following:

Yangmin Li and Qingsong Xu (2008). Design, Analysis and Applications of a Class of New 3-DOF Translational Parallel Manipulators, Parallel Manipulators, New Developments, Jee-Hwan Ryu (Ed.), ISBN: 978-3-902613-20-2, InTech, Available from:

http://www.intechopen.com/books/parallel_manipulators_new_developments/design__analysis_and_applications_of_a_class_of_new_3-dof_translational_parallel_manipulators

INTECH
open science | open minds

InTech Europe

University Campus STeP Ri
Slavka Krautzeka 83/A
51000 Rijeka, Croatia
Phone: +385 (51) 770 447
Fax: +385 (51) 686 166
www.intechopen.com

InTech China

Unit 405, Office Block, Hotel Equatorial Shanghai
No.65, Yan An Road (West), Shanghai, 200040, China
中国上海市延安西路65号上海国际贵都大饭店办公楼405单元
Phone: +86-21-62489820
Fax: +86-21-62489821

© 2008 The Author(s). Licensee IntechOpen. This chapter is distributed under the terms of the [Creative Commons Attribution-NonCommercial-ShareAlike-3.0 License](#), which permits use, distribution and reproduction for non-commercial purposes, provided the original is properly cited and derivative works building on this content are distributed under the same license.

IntechOpen

IntechOpen